Scanning Probe Microscopy

DOI: 10.1002/anie.201102796

Multifunctional Nanoprobes for Nanoscale Chemical Imaging and Localized Chemical Delivery at Surfaces and Interfaces**

*Yasufumi Takahashi, Andrew I. Shevchuk, Pavel Novak, Yanjun Zhang, Neil Ebejer, Julie V. Macpherson, Patrick R. Unwin, Andrew J. Pollard, Debdulal Roy, Charles A. Clifford, Hitoshi Shiku, Tomokazu Matsue, David Klenerman, and Yuri E. Korchev**

The dynamics of chemical and biological processes at interfaces underpin a wide range of phenomena, from surface adsorption and crystal growth to signal transduction at the cell membrane. Since many interfaces have nanoscale structures which control these phenomena, it is vital to be able to perform measurements of chemical and biochemical fluxes on this length scale. One technique with the potential to measure chemically specific fluxes on the nanoscale is scanning electrochemical microscopy (SECM),[1,2] but a lack of reliable distance (feedback) control (in contrast to other scanning probe microscopes) and difficulties in fabricating small-scale electrodes have largely restricted the technique to the microscale.[3] Electrochemical imaging on the nanoscale has been demonstrated only rarely[4] and in rather unusual environments.[5,6] There have been various attempts to introduce distance control into SECM by using, for example, shear force,[7–9] intermittent contact (IC) SECM,[10,11] SECM-AFM,[11–14] and the combination of SECM with scanning ion conductance microscopy (SICM).[15,16] While these techniques have the potential to allow electrochemical imaging on the nanoscale, they have the major disadvantage that they require specialist probes which are often difficult and time-consuming to fabricate and use.

Herein, we introduce an extremely quick (<2 min) and simple process with a high success rate for making double-barrel carbon nanoprobes (DBCNPs) for use in SECM-SICM. The overall probe radius is controllable on the nano- to microscale (see below), and the probes can be used for simultaneous chemical and topographical imaging, nanopositioning, and localized chemical delivery and detection by using SICM[17–20] distance feedback control. We first demonstrate its capability with approach curve measurements and by imaging test samples, and then by demonstrating its application to rat adrenal pheochromocytoma cells (PC12) by the simultaneous high-resolution imaging of the topography and electrochemical activity. Finally, exemplar studies of the localized chemical stimulation and detection of neurotransmitter release from PC12 cells by using DBCNPs is reported, which provides a platform for many future applications in cell biology.

DBCNPs were fabricated with one barrel filled with carbon for use as the SECM nanoelectrode, and the other barrel filled with electrolyte for SICM. The double-barrel pipette was pulled from a "theta" quartz capillary. This type of pipette was previously used for SICM and controlled deposition,[21,22] for the electrochemical imaging of electrode surfaces,[23] and for investigation of charge-transfer processes.[24] For SECM-SICM, one barrel was coated internally with carbon, formed in situ by the pyrolytic decomposition of butane;[25–27] the details of the fabrication method are described in the experimental section (Figure 1a). After carbon deposition, electrical contact was established by inserting a conductive wire through the top end of the pipette barrel to contact the carbon layer. The second barrel was unmodified, filled with electrolyte, and used for SICM distance control and chemical delivery (Figure 1b).

The method allows fabrication of DBCNPs with a radius ranging from 10 nm to 1 μm. Examples of field emission scanning electron microscopy (FESEM) images of different-sized electrodes are presented in Figure 1 and Figure S1 in the Supporting Information. The sizes of the DBCNPs are controlled by the initial capillary pulling process, and show high reproducibility; a typical size distribution of DBCNPs is shown in Figure S2 in the Supporting Information. The Supporting Information also contains exemplar studies of voltammetry at these probes, for a range of apparent sizes and

[*] Dr. Y. Takahashi, Dr. A. I. Shevchuk, Dr. P. Novak, Prof. Y. E. Korchev
Division of Medicine, Imperial College London
London W12 0NN (UK)
E-mail: y.korchev@ic.ac.uk
Prof. Y. Zhang
China National Academy of Nanotechnology & Engineering
Tianjin 300457 (China)
N. Ebejer, Prof. J. V. Macpherson, Prof. P. R. Unwin
Department of Chemistry, University of Warwick
Coventry CV4 7AL (UK)
Dr. A. J. Pollard, Dr. D. Roy, Dr. C. A. Clifford
National Physical Laboratory
Teddington TW11 0LW (UK)
Dr. H. Shiku, Prof. T. Matsue
Graduate School of Environmental Studies, Tohoku University
Aramaki Aoba 6-6-11-605, Sendai 980-8579 (Japan)
and
Advanced Institute of Materials Research, Tohoku University
Katahira, Aoba 2-1-1, Sendai 980-8577 (Japan)
Prof. D. Klenerman
Department of Chemistry, Cambridge University
Cambridge, CB2 1EW (UK)

[**] This work was funded by the EPSRC and the Chemical and Biological Programme of the National Measurement System of the UK Department of Business, Innovation, and Skills. Y.T. acknowledges support from JSPS Postdoctoral Fellowships for Research Abroad. P.R.U. thanks the European Research Council for support.

Supporting information for this article is available on the WWW under http://dx.doi.org/10.1002/anie.201102796.

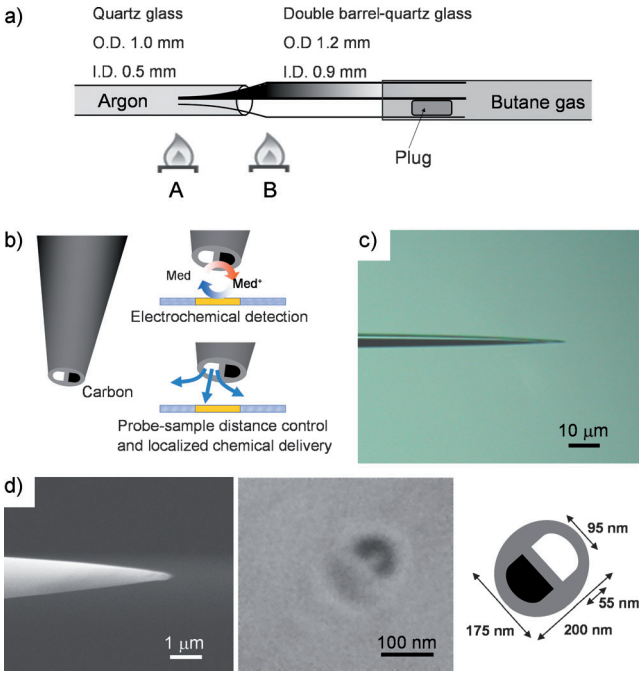

Figure 1. DBCNP fabricated by using the pyrolytic carbon deposition method. a) Schematic illustration of the fabrication method of the DBCNP. b) The principle of combined SECM-SICM measurement with a DBCNP. c) Optical microscopy image of the side view of the DBCNP. d) FESEM images of the side and top of the DBCNP. Note, the carbon deposited inside one of the barrels appears lighter compared to an empty barrel on the FESEM image, but is shown black in the schematic representation (a,b)

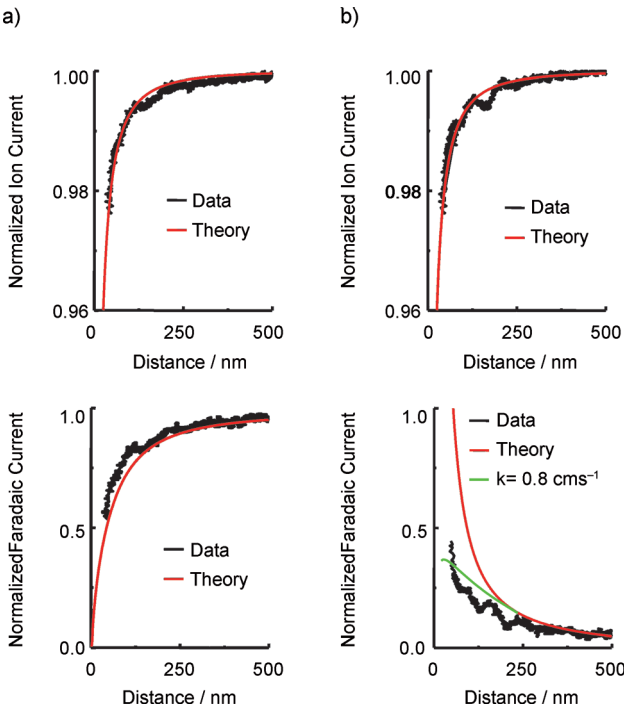

Figure 2. Approach curves of a DBCNP for simultaneous ion current (top) and electrochemical (bottom) measurements on an insulating (a) and conductive (b) substrate in 1.0 mM $FcCH_2OH$ + PBS. The SECM and SICM electrodes were held at 500 and 200 mV versus a reference Ag/AgCl electrode, respectively. The RG value used for the theoretical curves was 1.5.

redox couples, from simple electron transfer to ferrocenylmethanol ($FcCH_2OH$) to fast-scan cyclic voltammetry (FSCV) for the detection of dopamine (Figure S3).

Figure 1 c,d show optical and FESEM images of the apex of a typical DBCNP. In this particular case, the effective radii of the SICM aperture and SECM carbon electrode are less than 50 nm and the overall probe radius is only 100 nm. This provides an important advantage for the topographical and electrochemical imaging of cell surfaces, since the probe can access the cell surface and detect areas of slight roughness without unwanted probe-cell contact.[20]

Figure 2 a,b show typical experimental approach curves (black lines), for the SECM and SICM channels (recorded simultaneously), with insulating and conducting substrates, respectively. Both channels were fit to established theoretical curves for a simple disk geometry or opening[4,10,28–30] (red lines). This is found to provide a reasonable description of the basic characteristics of the probes, particularly given the idealized (single symmetric channel) of these models compared with the DBCNP geometry, and the fact that the latter will show some non-idealities on the nanoscale. As expected, the ion-current signal decreases for both the insulating and conducting substrates as the distance decreases, thereby highlighting that it can be used for unambiguous distance feedback control.

The SECM approach for the insulating and conducting substrates (Pt interdigitated array electrode (IDA)) showed negative (hindered diffusion) and positive (redox regeneration) feedback responses, respectively.[31] In this case, the electrode radius a was estimated to be 120 nm from the steady-state current in bulk solution and the fact that the negative feedback approach curve fits reasonably well to this value (and RG 1.5 (RG = ratio of the radii of the insulating sheath and the electrode)) indicates that the disks have a good planar geometry, as evident in the FESEM images. Furthermore, it is noteworthy that, by using the ion current feedback distance control, the electrode could approach the substrate as close as 50 nm without making direct contact. While one might expect to see pure positive feedback with an unbiased conductive surface, the experimental data indicate finite regeneration (surface redox) kinetics. Such effects have been seen previously with nanoscale tips at unbiased surfaces[4,10] and can be attributed to the fact that a small tip–substrate separation results in high mass transfer (D/d ca. 2 $cm\,s^{-1}$ at the closest separation d, where D is the diffusion coefficient of the redox species). The characteristic heterogeneous rate constant appears to be of the order of $k = 0.80\ cm\,s^{-1}$; deviations in the fit between experiment and theory can be attributed to non-ideality in the probe geometry.

Importantly, because the SICM channel provides the tip to surface distance, k is the only adjustable parameter when fitting the data. This highlights a key aspect of the SECM-SICM technique: the unambiguous quantitative determination of surface kinetics (and fluxes) because the distance between the tip and surface is known.

To evaluate the resolution of the DBCNP we recorded topographical and electrochemical images of nanopores (pore radii ca. 100 nm) in polyethylene terephthalate (PET) membranes. In our experiment, both sides of the membrane were filled with phosphate-buffered saline (PBS) containing 1.0 mM $FcCH_2OH$. The oxidation current of the $FcCH_2OH$ was recorded simultaneously with the topography by using the DBCNP ($a = 28$ nm); the potentials of the SECM carbon and SICM Ag/AgCl electrodes were 500 and 200 mV, respectively, for this and other test substrates. A constant d value of 30 nm was maintained by the SICM feedback. Figure 3a shows simultaneously recorded topographical and electrochemical images of the PET membrane, with the pore shapes and the electrochemical signals corresponding to the pore positions seen clearly. The decrease in the $FcCH_2OH$ oxidation current indicates that the diffusion of the $FcCH_2OH$ was blocked by the pore (decreased SECM channel current), because the probe moves towards the membrane under SICM feedback control as the probe encounters the pore.

To test the DBCNPs further, SECM-SICM was used to image a Pt IDA (Figure 3b). The d value was maintained at 100 nm by the SICM feedback, so that the SECM current clearly reflects the electrochemical activity of the sample. The oxidation current of the $FcCH_2OH$ was recorded simultaneously with the topography by using a DBCNP ($a = 88$ nm). It is clear that the electrochemical signal increases over the Pt bands (100 nm high in the SICM topography image) because of redox cycling, as for the approach curves in Figure 2c. Importantly, with this design of SECM-SICM probe, the insulation is considerably better (there are no pinholes or recessing of the electrode) and the probe size is smaller than previously reported.[15]

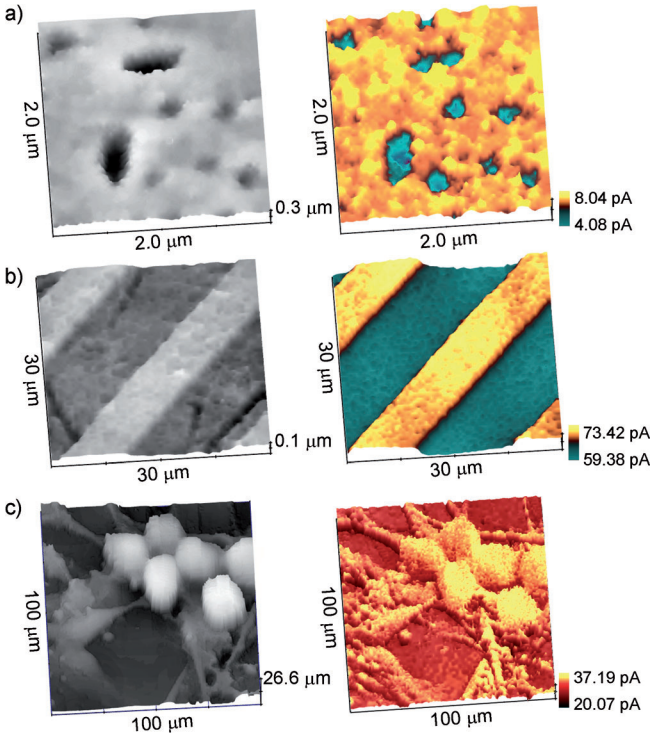

Figure 3. Simultaneous topographical (left) and electrochemical (right) images. a) PET in 1.0 mM $FcCH_2OH$ + PBS. b) Pt interdigitated array in 1.0 mM $FcCH_2OH$ + PBS. c) Living sensory neurons in 0.5 mM $FcCH_2OH$ + HBSS. The SECM and SICM electrodes were held at 500 and 200 mV versus a reference Ag/AgCl electrode, respectively. Electrochemical images were based on an oxidation current of $FcCH_2OH$.

To demonstrate electrochemical and topographical imaging of neurons using DBCNPs ($a = 240$ nm) we visualized the permeation of $FcCH_2OH$, a hydrophobic mediator which can cross the cell membrane, simultaneously with the topography of living sensory neurons. Figure 3c shows the SECM-SICM images of sensory neurons in Hank's buffered salt solution (HBSS) containing 0.5 mM $FcCH_2OH$. The tall cell bodies, exceeding 25 μm in height, and dendritic structures are clearly observed in both the SICM and SECM images, which correlate very well. The SICM images represent the topography, whereas the SECM images measure the flux of $FcCH_2OH$. When the probe is over the bare petri dish, a current of 23 pA is typically recorded, which is the value expected for hindered diffusion. In contrast, when the probe is over the cells, an enhanced current is observed, which approaches the value of 38 pA when the probe is in bulk solution. This finding indicates that the cellular membrane is permeable to $FcCH_2OH$ and that the permeability can be visualized, largely free from topographical effects, because of the independent distance control from SICM. Furthermore, the electrochemical response shows no deterioration in this biological medium. Thus, the DBCNP can be used for localized electrochemical measurements and simultaneous imaging of the surface topography of complex live biological samples.

To further validate the capabilities of SECM-SICM for imaging the topography of living cells we compared the topography of differentiated PC12 cells by using both a DBCNP and a single SICM nanopipette (Figure 4a,b respectively). The topography of neurons[7,32] and release of neurotransmitters have been previously investigated by using shear force distance control SECM[7] and SICM.[32] However, the resolution of these measurements was not sufficient to probe the dendritic structure of the neuron in any detail. In this present study, the radii of the SICM aperture of the DBCNP and the SICM nanopipette were both 50 nm. The quality of the topographic images were comparable: similar dendritic structures, less than 200 nm diameter, were observed on both images (Figure 4a,b, white arrows).

To enhance the sensitivity of the electrochemical detection by the DBCNPs to enable the release of neurotransmitters to be detected it is important to increase the carbon surface area, but not the SICM barrel aperture for distance feedback control. We thus fabricated cylindrically shaped DBCNPs by depositing additional carbon on the outside of the pipette. The method for depositing carbon on the outer surface of the micropipette tip was as described previously,[27] such that the steady-state current measured in 1 mM $FcCH_2OH$ and PBS was 1.85 nA. We then measured the release of neurotransmitter from undifferentiated PC12 cells with this type of probe (Figure 5a). The FESEM image was taken at a tilted angle to show the deposited carbon on the outside of the capillary. A key advantage of the DBCNP is

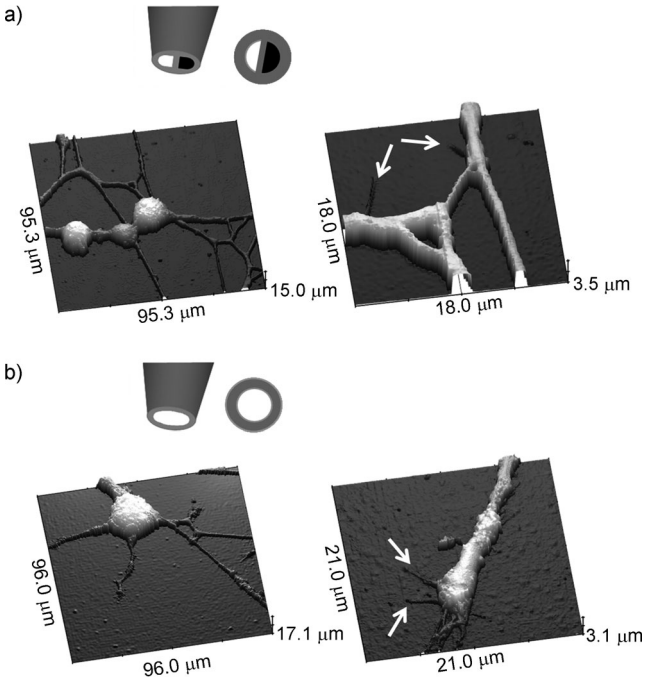

Figure 4. Nanoscale topography images of differentiated PC12 cells using a) the DBCNP and b) a single SICM nanopipette. The arrows showed the dendritic structures.

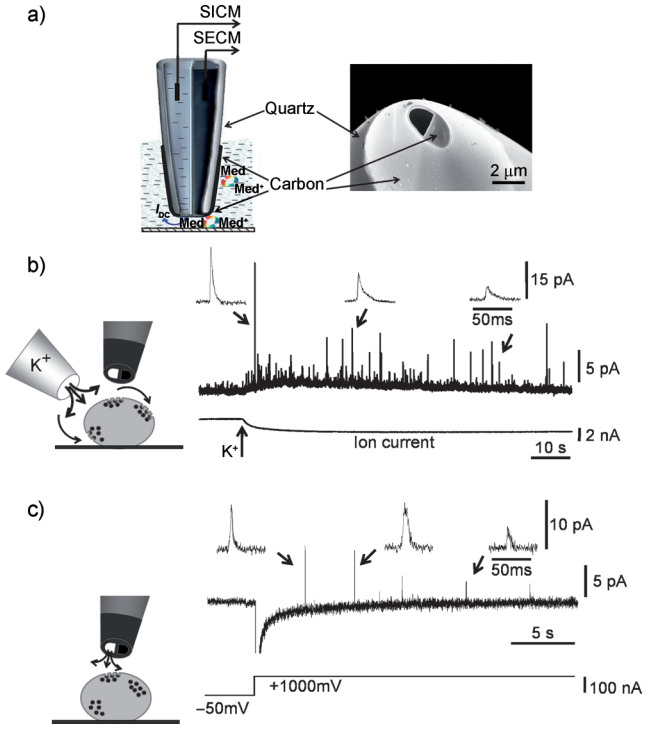

Figure 5. Detection of the release of the neurotransmitter by using the cylindrically shaped DBCNP. a) SEM image of a cylindrically shaped DBCNP. A series of current spikes corresponding to neurotransmitter release detected after b) whole cell stimulation with 105 mM K^+ using another micropipette and c) voltage-driven delivery of K^+ ions using a DBCNP. The carbon electrode was held at 650 mV versus a reference Ag/AgCl electrode.

that it can be positioned with very high precision by using the SICM control: in the present studies it was positioned 500 nm above a PC12 cell.

To stimulate neurotransmitter release we depolarized a PC12 cell by stimulation of the whole cell with 105 mM K^+ by using another micropipette ($a = 3$ μm). Figure 5b shows a series of current spikes corresponding to release of the neurotransmitter which was detected by the probe. The insets of Figure 5b show expanded views of the releasing signal, where the amplitudes and the widths of the spike are clearly visible. It was shown previously that the amplitude and shape of the signal was dependent on the separation between the electrode and release site.[33] It is also possible to observe the increase in local K^+ concentration at the DBCNP by the increase in the negative ion current (Figure 5b, bottom trace).

One of the great advantages of using DBCNPs is that the barrel filled with electrolyte can be used to apply different reagents for local stimulation of the cell: the voltage-driven local chemical change produced by the nanopipette is effective for controlling the function of the biological sample.[34] Therefore, in the next series of experiments we performed voltage-driven application of K^+ ions by using the DBCNP itself to achieve both the local depolarization of the cell membrane and simultaneous detection of the neurotransmitter. With the SICM barrel filled with 3 M KCl, the applied voltage of the SICM electrode was changed from −50 mV to 1000 mV. This ejected potassium ions from the SICM barrel pipette towards the cell surface, thereby inducing local triggering of neurotransmitter release. Figure 5c shows a series of current spikes that were detected after local stimulation with the voltage-driven application of K^+ ions.

With local stimulation we always detected either a low frequency of current spikes compared with whole cell stimulation or no spikes at all. This finding suggests that the DBCNP can be used to induce and detect localized release of the neurotransmitter over the cell surface, thus opening up possibilities to perform the mapping of neurotransmitter release sites.

We have developed a simple, affordable, and quick method of fabricating a DBCNP for functional nanoscale (electro)chemical imaging by using SICM distance feedback control. The fabrication method yields probes with controllable radii in the range of 10 nm to 1 μm with excellent temporal and spatial resolution. Among the many possibilities in the physical and life sciences, this novel probe allows the mapping of sites of neurotransmitter release together with the associated changes in the cell topography that occur during exocytosis, and in the future this technique could be extended to perform intracellular measurements.

Experimental Section

For fabrication of the DBCNP, a quartz theta glass capillary (O.D. 1.2 mm, I.D. 0.9 mm; Sutter Instrument, USA) was pulled using a CO_2 laser puller (model P-2000, Sutter Instrument, San Rafael, CA, USA). Figure 1a shows a schematic illustration of the fabrication system. Butane was passed through the quartz capillary by using a Tygon tube (O.D. 2.4 mm, I.D. 0.8 mm). First, both of the ends of the barrels were blocked with reusable putty-like pressure-sensitive adhesive. Next, one of the barrels was opened and pressurized with butane gas to

deposit carbon inside this barrel only. The other barrel remained blocked and, therefore, no carbon was deposited so that it could be used for SICM. The taper of the pipette was inserted into another quartz capillary (O.D. 1.0 mm, I.D. 0.7 mm; Sutter Instrument, USA), which was filled with argon gas to prevent oxidation of the carbon layer and bending of the capillary by high temperature. This approach also protected the pipette aperture from closing through softening of the quartz pipette walls. To form a pyrolytic carbon layer inside the capillary, the pipette taper was then heated with a Bunsen burner for times ranging from 0.5 s for a 100 nm radius electrode through to 3 s for a 1 μm radius electrode. The deposited layer of carbon inside the pipette is clearly observed in the SEM image of a cross-section of a DBCNP shown in Figure S1c.

To detect release of the neurotransmitter from a PC12 cell, an increase in the carbon surface area was required for enhanced sensitivity of the electrochemical measurement. We, therefore, fabricated cylindrically shaped DBCNPs by depositing carbon on the outside of the top of the tip. Details of the deposition have been described in a previous report.[27] The argon flow ($1.2\,L\,min^{-1}$) is important to control the outside area of carbon deposition. Additionally, the activation of the carbon electrode is also an important process for the detection of neurotransmitters.[35] The DBCNPs were activated by applying −1.0 V versus a reference Ag/AgCl electrode for 1 min.

The DBCNP was difficult to fill with the electrolyte solution because of air plugs that formed close to the pipette taper. To force these air bubbles out of the electrolyte we used a cigarette gas lighter to quickly heat the solution inside the pipette. The heat supplied by the gas lighter was not great enough to soften the quartz walls of the pipette, but resulted in rapid expansion of the air bubble and its movement towards the wider part of the pipette, thereby unblocking the pipette tip. This allowed reliable filling of the pipette with electrolyte.

The SECM-SICM instrument used was similar to one previously described[15] and was operated in a hopping mode.[20] Details of the SECM-SICM instrument, chemicals and materials, and preparation of the cell culture are described in the supporting information.

Received: April 21, 2011
Revised: July 14, 2010
Published online: September 1, 2011

Keywords: biosensors · living cell imaging · nanoelectrodes · scanning probe microscopy · surface analysis

[1] A. Schulte, W. Schuhmann, *Angew. Chem.* **2007**, *119*, 8914; *Angew. Chem. Int. Ed.* **2007**, *46*, 8760.
[2] G. Wittstock, M. Burchardt, S. E. Pust, Y. Shen, C. Zhao, *Angew. Chem.* **2007**, *119*, 1604; *Angew. Chem. Int. Ed.* **2007**, *46*, 1584.
[3] S. Amemiya, A. J. Bard, F. R. F. Fan, M. V. Mirkin, P. R. Unwin, *Annu. Rev. Analyt. Chem.* **2008**, *1*, 95.
[4] F. O. Laforge, J. Velmurugan, Y. X. Wang, M. V. Mirkin, *Anal. Chem.* **2009**, *81*, 3143.
[5] F. R. F. Fan, A. J. Bard, *Proc. Natl. Acad. Sci. USA* **1999**, *96*, 14222.
[6] J. V. Macpherson, P. R. Unwin, *Anal. Chem.* **2000**, *72*, 276.
[7] A. Hengstenberg, A. Blochl, I. D. Dietzel, W. Schuhmann, *Angew. Chem.* **2001**, *113*, 942; *Angew. Chem. Int. Ed.* **2001**, *40*, 905.
[8] Y. Takahashi, Y. Hirano, T. Yasukawa, H. Shiku, H. Yamada, T. Matsue, *Langmuir* **2006**, *22*, 10299.
[9] Y. Takahashi, T. Miyamoto, H. Shiku, R. Asano, T. Yasukawa, I. Kumagai, T. Matsue, *Anal. Chem.* **2009**, *81*, 2785.
[10] K. McKelvey, M. A. Edwards, P. R. Unwin, *Anal. Chem.* **2010**, *82*, 6334.
[11] A. Kueng, C. Kranz, A. Lugstein, E. Bertagnolli, B. Mizaikoff, *Angew. Chem.* **2003**, *115*, 3358; *Angew. Chem. Int. Ed.* **2003**, *42*, 3238.
[12] D. P. Burt, N. R. Wilson, J. M. R. Weaver, P. S. Dobson, J. V. Macpherson, *Nano Lett.* **2005**, *5*, 639.
[13] C. E. Gardner, P. R. Unwin, J. V. Macpherson, *Electrochem. Commun.* **2005**, *7*, 612.
[14] A. Ueda, O. Niwa, K. Maruyama, Y. Shindo, K. Oka, K. Suzuki, *Angew. Chem.* **2007**, *119*, 8386; *Angew. Chem. Int. Ed.* **2007**, *46*, 8238.
[15] Y. Takahashi, A. I. Shevchuk, P. Novak, Y. Murakami, H. Shiku, Y. E. Korchev, T. Matsue, *J. Am. Chem. Soc.* **2010**, *132*, 10118.
[16] D. J. Comstock, J. W. Elam, M. J. Pellin, M. C. Hersam, *Anal. Chem.* **2010**, *82*, 1270.
[17] P. K. Hansma, B. Drake, O. Marti, S. A. C. Gould, C. B. Prater, *Science* **1989**, *243*, 641.
[18] Y. E. Korchev, C. L. Bashford, M. Milovanovic, I. Vodyanoy, M. J. Lab, *Biophys. J.* **1997**, *73*, 653.
[19] A. I. Shevchuik, G. I. Frolenkov, D. Sanchez, P. S. James, N. Freedman, M. J. Lab, R. Jones, D. Klenerman, Y. E. Korchev, *Angew. Chem.* **2006**, *118*, 2270; *Angew. Chem. Int. Ed.* **2006**, *45*, 2212.
[20] P. Novak, C. Li, A. I. Shevchuk, R. Stepanyan, M. Caldwell, S. Hughes, T. G. Smart, J. Gorelik, V. P. Ostanin, M. J. Lab, G. W. Moss, G. I. Frolenkov, D. Klenerman, Y. E. Korchev, *Nat. Methods* **2009**, *6*, 279.
[21] K. T. Rodolfa, A. Bruckbauer, D. J. Zhou, Y. E. Korchev, D. Klenerman, *Angew. Chem.* **2005**, *117*, 7014; *Angew. Chem. Int. Ed.* **2005**, *44*, 6854.
[22] K. T. Rodolfa, A. Bruckbauer, D. J. Zhou, A. I. Schevchuk, Y. E. Korchev, D. Klenerman, *Nano Lett.* **2006**, *6*, 252.
[23] N. Ebejer, M. Schnippering, A. W. Colburn, M. A. Edwards, P. R. Unwin, *Anal. Chem.* **2010**, *82*, 9141.
[24] H. Hu, S. Xie, X. Meng, P. Jing, M. Zhang, L. Shen, Z. Zhu, M. Li, Q. Zhuang, Y. Shao, *Anal. Chem.* **2006**, *78*, 7034.
[25] Y. T. Kim, D. M. Scarnulis, A. G. Ewing, *Anal. Chem.* **1986**, *58*, 1782.
[26] D. K. Y. Wong, L. Y. F. Xu, *Anal. Chem.* **1995**, *67*, 4086.
[27] M. McNally, D. K. Y. Wong, *Anal. Chem.* **2001**, *73*, 4793.
[28] J. L. Amphlett, G. Denuault, *J. Phys. Chem. B* **1998**, *102*, 9946.
[29] M. A. Edwards, C. G. Williams, A. L. Whitworth, P. R. Unwin, *Anal. Chem.* **2009**, *81*, 4482.
[30] Y. H. Shao, M. V. Mirkin, *J. Phys. Chem. B* **1998**, *102*, 9915.
[31] J. Kwak, A. J. Bard, *Anal. Chem.* **1989**, *61*, 1794.
[32] S. A. Mann, G. Hoffmann, A. Hengstenberg, W. Schuhmann, I. D. Dietzel, *J. Neurosci. Methods* **2002**, *116*, 113.
[33] R. M. Wightman, T. J. Schroeder, J. M. Finnegan, E. L. Ciolkowski, K. Pihel, *Biophys. J.* **1995**, *68*, 383.
[34] J. D. Piper, C. Li, C. J. Lo, R. Berry, Y. Korchev, L. M. Ying, D. Klenerman, *J. Am. Chem. Soc.* **2008**, *130*, 10386.
[35] F. G. Gonon, C. M. Fombarlet, M. J. Buda, J. F. Pujol, *Anal. Chem.* **1981**, *53*, 1386.

